

Solar Wakes of Dark Matter Flows

Pierre Sikivie and Stuart Wick

Department of Physics, University of Florida, Gainesville, FL, 32611

March 25, 2002

Abstract

We analyze the effect of the Sun's gravitational field on a flow of cold dark matter (CDM) through the solar system in the limit where the velocity dispersion of the flow vanishes. The exact density and velocity distributions are derived in the case where the Sun is a point mass. The results are extended to the more realistic case where the Sun has a finite size spherically symmetric mass distribution. We find that regions of infinite density, called caustics, appear. One such region is a line caustic on the axis of symmetry, downstream from the Sun, where the flow trajectories cross. Another is a cone-shaped caustic surface near the trajectories of maximum scattering angle. The trajectories forming the conical caustic pass through the Sun's interior and probe the solar mass distribution, raising the possibility that the solar mass distribution may some day be measured by a dark matter detector on Earth. We generalize our results to the case of flows with continuous velocity distributions, such as that predicted by the isothermal model of the Milky Way halo.

PACS number: 98.80 Cq

I. INTRODUCTION

There are compelling reasons to believe that the dark matter of the universe is constituted in large part of non-baryonic collisionless particles with very small primordial velocity dispersion [1]. Generically, such particles are called cold dark matter (CDM). The leading CDM candidates are the axion and the lightest supersymmetric partner in supersymmetric extensions of the Standard Model of elementary particles. The latter candidate is a weakly interacting massive (mass in the 10 to 100 GeV range) particle, or WIMP for short. The former has mass in the 10^{-5} to 10^{-6} eV range and is extremely weakly interacting, so weakly in fact that it was once thought “invisible”.

Wherever a galaxy forms, the surrounding CDM falls into the galactic gravitational potential. Unlike baryons, CDM is collisionless and sloshes back and forth in the potential well, producing a galactic halo of size much larger than the extent of the visible matter. The local (i.e., on Earth) dark matter density of the Milky Way halo is of order 10^{-24} gr/cm³. This local dark matter is in principle detectable and considerable effort is being spent on projects devoted to this goal. Dark matter axions can be detected by their conversion to microwave photons in an electromagnetic cavity permeated by a strong static magnetic field [2]. WIMPs can be detected by observing the recoil energy of nuclei off which WIMPs have scattered elastically [3,4]. WIMP dark matter may also be detected indirectly by observing, on Earth, neutrinos produced in the annihilation of WIMPs which accumulated in the interior of the Sun [5].

From the point of view of these dark matter searches it is desirable to know as much as possible about the phase-space distribution $f(\vec{r}, \vec{v})$ of CDM in galactic halos in general, and particularly in the Milky Way halo. One wants to know not only the local density but also the local velocity distribution. In the cavity dark matter axion detector, the kinetic energy spectrum of dark matter axions can be measured with great resolution [2]. Knowledge of the velocity distribution may therefore be exploited to increase the sensitivity of the search. In WIMP searches, knowledge of the velocity spectrum is necessary to calculate the annual modulation of the signal [6]. This annual modulation is an important means by which the signal to background ratio can be enhanced.

Yet, in spite of this urgent need of the ongoing cold dark matter searches, there is at present no consensus about the phase-space structure of galactic halos. Let us discuss briefly the three main approaches which have been put forth.

The oldest description of galactic halos is the isothermal model [7]. It postulates that the phase-distribution is given by Boltzmann’s law, the energy of each particle being its kinetic energy plus its gravitational potential energy in the presence of all the other particles. It can be shown that the dark matter density then falls off as $d(r_G) \propto \frac{1}{r_G^2}$ for large values of the galactocentric distance r_G . Therefore the model predicts that galactic rotation curves are flat ($v(r_G) \propto \text{constant}$) at large r_G , and that is indeed what is observed. Another virtue of the model is that it predicts that at small r_G , within some radius called the core radius a , the density d goes to a constant, and hence that the halo contribution to galactic rotation curves $v_{\text{halo}}(r_G) \propto r_G$ at small r_G . That also is consistent with observation. The model predicts all properties of galactic halos in terms of just two parameters: the velocity dispersion $\sqrt{\bar{v}^2}$ and the core radius a . In fits to observed properties of our own halo, $\sqrt{\bar{v}^2}$ is found to be

approximately 270 km/s and a of order several kpc.

The isothermal model is simple and gives an excellent overall description of what is observed, but there is little justification for its basic assumption, that the dark matter particles in galactic halos are thermalized. Thermalization may have occurred during an early phase of 'violent relaxation' [8] at the time of collapse of the protogalaxy. It is possible that the dark matter that fell onto the Galaxy at early times was thermalized by that process. But an isolated galaxy such as the Milky Way is still accreting dark matter today because it is surrounded by a sea of dark matter. (The presence of M31 and the other members of the local group is not relevant for the purpose of this discussion.) There is no evidence of violent relaxation occurring in the Galaxy at the present time. The infalling dark matter particles form flows which slosh back and forth in the gravitational potential of the galaxy. The flows do not get thermalized over the age of the universe [9]. Gravitational scattering by inhomogeneities, such as globular clusters and molecular clouds, is too weak to diffuse the flows entirely, except for those flows which always remained within the inner parts ($r_G \lesssim 20$ kpc, say) of the Galaxy.

The flows can be described in terms of the evolution of the 3-dim. sheet on which the dark matter particles lie in 6-dim. phase-space [9]. Before the onset of galaxy formation, the equation of the sheet is $\vec{v} = H(t)\vec{r} + \Delta\vec{v}(\vec{r}, t)$ where $H(t)$ is the Hubble expansion rate and $\Delta\vec{v}(\vec{r}, t)$ is the peculiar velocity field associated with density perturbations. The thickness of the sheet is the primordial velocity dispersion δv . The primordial velocity dispersion of the leading cold dark matter candidates is extremely small, of order $10^{-12}c$ for WIMPs and $3 \cdot 10^{-17}c$ (at most) for axions. The sheet cannot tear and hence its evolution is constrained by topology. Where a galaxy forms, the sheet wraps up in phase-space, turning clockwise in any two dimensional cut (x, \dot{x}) of that space. x is the physical space coordinate in an arbitrary direction and \dot{x} is the associated velocity. The outcome of this process is a discrete set of flows at any point in a galactic halo. Two flows are associated with particles falling in and out of the galaxy for the first time ($n = 1$), two other flows are associated with particles falling in and out of the galaxy for the second time ($n = 2$), and so on. The number of such flows at the Earth's location in the Milky Way is of order 100 [9]. The flows of particles which have fallen in and out of the Galaxy only a small number of times in the past ($n \lesssim 20$) are not expected to be thermalized. The flows with larger n may be thermalized because they are composed of particles which fell in a long time ago.

Caustics appear wherever the projection of the phase-space sheet onto physical space has a fold [10–12]. Caustics are generically surfaces in physical space. On one side of the surface there are two more flows than on the other. At the surface, the dark matter density is very large. It diverges there in the limit of zero velocity dispersion. There are two types of caustics in the halos of galaxies, inner and outer. The outer caustics are topological spheres surrounding the galaxy. They are located near where a given outflow reaches its furthest distance from the galactic center before falling back in, and are described by A_2 (or 'fold') catastrophes. The inner caustics are rings [10]. They are located near where the particles with the most angular momentum in a given inflow reach their distance of closest approach to the galactic center before going back out. A caustic ring is a closed tube whose cross-section is a D_{-4} (also called *elliptic umbilic*) catastrophe [12]. The existence of these caustics and their topological properties are independent of any assumptions of symmetry.

A second approach to describing the structure of galactic halos is in terms of these flows and their associated caustics [9,13,10,14,12,15,16]. Let us call that approach the 'caustic ring model' since caustic rings are one of its prominent features. In the model the caustic ring radii, and indeed the whole phase-space distribution, are calculated assuming that halo formation is a self-similar process [17,13]. The model depends on only three parameters: the galactic rotation velocity v_{rot} , a parameter j_{max} which is proportional to the amount of angular momentum in the halo, and a parameter ϵ which describes the profile of the initial overdensity from which the galaxy forms. ϵ is related to the slope of the evolved power spectrum of primordial density perturbations and hence, to the extent that that spectrum is predicted by CDM cosmology, ϵ is not a free parameter. If the primordial spectrum is Harrison-Zel'dovich, ϵ is in the range 0.2 to 0.35. [13]. In that range, the self-similar model predicts that the density $d(r_G) \propto \frac{1}{r_G^2}$ at large r_G . Hence the model predicts that galactic rotation curves are flat at large r_G , which is consistent with observation. When $j_{\text{max}} = 0$, the $d(r_G) \propto \frac{1}{r_G^2}$ behavior extends to small r_G . The $\frac{1}{r_G^2}$ singularity at $r_G = 0$ is due to the fact that the dark matter particles move on radial orbits in that limit. However, the dark matter particles are expected to carry angular momentum. When $j_{\text{max}} \neq 0$, the density is depleted within an effective core radius r_c . As a result, the halo contribution $v_{\text{halo}}(r_G)$ to the rotation curve goes to zero as $r_G \rightarrow 0$, which is also consistent with observation.

Evidence for the presence of caustic rings in our galaxy was found in the distribution of rises in the Milky Way rotation curve, and in a triangular feature in an IRAS map of the galactic disk [16]. The feature is reminiscent of the shape of the D_{-4} catastrophe. When the model is fitted to these observations, its parameters are determined to be: $v_{\text{rot}} \simeq 220$ km/s, and $j_{\text{max}} \simeq 0.26$ for $\epsilon = 0.3$. The model predicts the dark matter flows and caustics in the solar neighborhood. Because of our proximity to the fifth caustic ring, one of the flows dominates over all others combined. Its density and velocity vector (known only up to a two-fold ambiguity) relative to the non-rotating restframe of the Galaxy are [16]:

$$d_5^+ = 1.7 \cdot 10^{-24} \frac{\text{gr}}{\text{cm}^3}, \quad \vec{v}_5 = (470 \hat{\phi}_G \pm 100 \hat{r}_G) \frac{\text{km}}{\text{s}} . \quad (1.1)$$

\hat{r}_G is the local unit vector in the direction away from the galactic center, and $\hat{\phi}_G$ is in the direction of galactic rotation. A list of the other flows is given in ref. [14]. The caustic ring model describes the minimum phase-space structure that a galactic halo must have. The actual phase-space structure cannot be simpler than that.

A third approach to studying the structure of galactic halos is by means of N-body simulations [18]. Initial density perturbations are chosen according to a theoretically expected probability distribution, e.g. Gaussian density perturbations with the CDM power spectrum evolved from a flat Harrison-Zel'dovich primordial spectrum. Overdensities grow in the simulations and form structures which are identified with galactic halos. In the large N limit, the outcome of the simulations can be identified with the predictions of CDM cosmology. However, present constraints on computing power restrict N to be of order 10^6 per galactic halo. In contrast, the number of axions per galactic halo is of order 10^{84} , and the number of WIMPs of order 10^{68} . Since phase-space is 6-dim. , the resolving power of the simulations is only a factor of ten in each dimension, including the three physical space dimensions. The simulations do show that galactic halos are not thermalized and that they contain discrete

flows. However, the limited resolution allows only a few flows to be seen. The simulations predict that a large galaxy like our own has hundreds of satellites. The tidal disruption of these satellites produces low velocity dispersion streams [19] which are in effect localized flows.

The purpose of this paper is to analyze the effect of the Sun's gravitational field on a flow of collisionless dark matter through the solar system. This effect was analyzed several years ago by K. Griest [20] in the case of the isothermal model. He calculated the annual modulation of the signal in WIMP detectors including the effects both of the Earth's orbital motion and the Sun's gravity. Earlier discussions of the effect of the Sun's gravity on a flow of ordinary collisionful matter can be found in papers by H. Bondi and F. Hoyle [21], J.M.A. Danby and G.L. Camm [22], and Danby and T.A. Bray [23]. We will study mainly the effect of the Sun's gravity on a single flow of collisionless dark matter in the limit of zero velocity dispersion. The effect of finite velocity dispersion can be taken account by integrating over a distribution of initial velocities. Our results can be applied to the calculation of the annual modulation of the signals in both the axion and WIMP dark matter detectors. We plan to do this in detail in a subsequent paper which will be concerned with the experimental implications of the present investigation. In the remainder of this Introduction, we give a general discussion of the annual modulation of the signal in the axion and WIMP detectors, including the role of the Sun's gravity.

A flow produces a peak in the energy spectrum of photons produced by axion \rightarrow photon conversion in the cavity detector of dark matter axions [2]. The peak's frequency ω is determined by the energy conservation relation, $\hbar\omega = m_a(c^2 + \frac{1}{2}v_{\text{flow} \div \text{lab}}^2)$, in terms of the flow speed relative to the laboratory. Because the Earth rotates, there is a diurnal modulation of the peak's frequency. By measuring the average frequency and the amplitude and phase of the modulation, one can derive the velocity vector $\vec{v}_{\text{flow} \div \oplus}$ of the flow relative to the Earth (\oplus). The height of the peak is proportional to the flow density.

On top of the diurnal modulation, there is a much larger annual modulation because the Earth orbits the Sun (\odot):

$$\hbar\bar{\omega}(t) = m_a[c^2 + \frac{1}{2}(\vec{v}_{\text{flow} \div \oplus}(t))^2] = m_a[c^2 + \frac{1}{2}(\vec{v}_{\text{flow} \div \odot}(t) - \vec{v}_{\oplus \div \odot}(t))^2] \quad , \quad (1.2)$$

where $\bar{\omega}$ is the peak frequency averaged to remove the diurnal modulation. $\vec{v}_{\oplus \div \odot}(t)$ follows from the Earth's orbital motion. Eq. (1.2) then gives $\bar{\omega}(t)$ in terms of $\vec{v}_{\text{flow} \div \odot}$, the flow velocity relative to the Sun. However, galactic halo models give the velocity \vec{v}_∞ of the flow long before it reaches the Sun. For example, for the 'big flow' of Eq. (1.1), $\vec{v}_\infty = \vec{v}_5 - \vec{v}_\odot$ where \vec{v}_\odot is the velocity of the Sun relative to the Galaxy. $\vec{v}_{\text{flow} \div \odot}$ differs from \vec{v}_∞ because the flow is affected by the gravitational field of the Sun. The relationship between \vec{v}_∞ and $\vec{v}_{\text{flow} \div \odot}$ depends on position and hence, as the Earth orbits the Sun, on time.

One of the main goals of this paper is to derive this relationship. Note that a single flow of velocity \vec{v}_∞ far from the Sun, produces more than one flow in the vicinity of the Sun. We call $n(\vec{r})$ the number of flows at position \vec{r} . We want to calculate $\vec{v}_{\text{flow} \div \odot, j}(\vec{r})$ for each of the flows $j = 1 \dots n(\vec{r})$. We also want to calculate the density $d_j(\vec{r})$ of each of the flows.

The simplest case is when the Sun is treated as a point mass. Then, $n = 2$ everywhere. Indeed there are two different ways in which particles coming with velocity \vec{v}_∞ from far away can reach an arbitrary location \vec{r} . See Fig. 1. We will find a caustic line downstream of

the Sun, on the positive z -axis if \hat{z} is the unit vector in the direction of \vec{v}_∞ . Indeed, every trajectory passes by some point on the positive z -axis; the latter is a focal line. We will see that the density diverges there as $\frac{1}{\rho}$ where ρ is the distance to the z -axis. We call this caustic the 'spike'.

In reality the Sun has finite radius. This implies that there is a maximum scattering angle $\Theta_{\max}(v_\infty) < 180^\circ$. As a result, at large distance r from the Sun, $n = 1$ for $\theta > \Theta_{\max}$ and $n = 3$ for $\theta < \Theta_{\max}$, where θ is the polar angle relative to the direction of $\vec{v}_\infty = \hat{z}v_\infty$. On the conical surface which separates the $n = 1$ and $n = 3$ regions, there is a caustic, which we call the 'skirt'. The spike caustic along the z -axis downstream from the Sun remains as in the point mass case. As the Earth moves around the Sun, it may come close to the spikes associated with some of the flows and it will go through many of their skirts. When it approaches these caustics, the density becomes larger. We will see that the profile of the skirt caustic is a functional of the mass distribution inside the Sun. We may optimistically envisage a time where the axion dark matter detector on Earth, monitoring the peak sizes associated with various flows, provides information about the solar mass distribution.

WIMP detectors measure the nuclear recoil energy when a WIMP scatters elastically off a nucleus in the detector [3,4]. The events caused by a single flow of WIMPs produce a plateau in the distribution of measured recoil energies. The edge of the plateau is at the highest recoil energy compatible with the kinetic energy of the WIMP. The highest recoil energy occurs when the collision is back-to-back in the center of mass. It is therefore a simple function of the mass of the nucleus, the mass of the WIMP and the speed of the WIMP in the laboratory frame. In principle, a WIMP detector can measure the speed of each of the flows by measuring the edge of the corresponding plateau in the recoil energy distribution. If the detector has directionality [24], it may determine the directions of the flows as well as their speeds.

All WIMP detectors are presently sensitive to the local dark matter velocity distribution through the annual modulation effect [6]. The event rate in a WIMP detector is proportional to the flux of WIMPs through the detector. (In contrast, the axion to photon conversion rate in the cavity detector of dark matter axions is proportional to the density of axions, not their flux.) The WIMP flux changes in the course of the year as the velocity of the Earth's orbital motion around the Sun adds to or subtracts from the velocity of the Sun with respect to the galactic halo.

Interestingly, the annual modulation effect in WIMP detectors distinguishes between the isothermal and caustic ring models of the Galaxy. In the isothermal model, the halo has zero average velocity everywhere. It has no net angular momentum, no rotation. The Sun moves with velocity of order 220 km/s in the direction $\hat{\phi}_G$ of the galactic disk rotation. The Earth moves with speed 30 km/s around the Sun in a plane, called the ecliptic, inclined at approximately 60° relative to $\hat{\phi}_G$. The direction of $\vec{v}_{\oplus \div \odot}$ is closest to $\hat{\phi}_G$ on about June 2. The WIMP flux, and hence the signal in a WIMP detector, is highest then. It is lowest six months later, near December 2. The amplitude of the modulation is of order $\cos(60^\circ) \frac{30 \text{ km/s}}{220 \text{ km/s}} \simeq 7\%$. In the caustic ring model, on the other hand, the halo does have net angular momentum. The locally dominant flows, such as Eq. (1.1), have velocity components in the $\hat{\phi}_G$ direction of order 470 km/s, more than twice the velocity of the Sun in that direction. Relative to the Sun, the average flow of dark matter is in the $+\hat{\phi}_G$ direction in the caustic ring model, whereas it is in the $-\hat{\phi}_G$ direction in the isothermal model. So the annual modulation in the

caustic ring model [14,25–27] has opposite sign to that of the isothermal model: the event rate in WIMP detectors is largest near December 2, lowest near June 2. Non-isothermal galactic halo models other than the caustic ring model are discussed in ref. [28].

The DAMA experiment in the Gran Sasso laboratory claims to have observed the annual modulation of the WIMP signal [29]. The DAMA results are consistent with the prediction of the isothermal model, and inconsistent with the caustic ring model. However, almost all of the region of WIMP mass and elastic scattering cross-section space implied by the DAMA signal is ruled out by the null result of the CDMS dark matter search [30]. Some of the region is also ruled out by the null result of the EDELWEISS experiment [31].

At any rate, it is clear that the annual modulation is an important way to distinguish signal from background in WIMP searches, and that it deserves the best possible theoretical treatment. Most calculations and discussions neglect the effect of the Sun’s gravity. However, as we mentioned already, the Sun’s gravity effect was analyzed by K. Griest for the case of the WIMP signal in the isothermal model [20]. In that model the flow of dark matter relative to the Sun produces a wake in the $-\hat{\phi}_G$ direction. We may think of it as a spike caustic except that it is spread out in space because of the large velocity dispersion ($\sqrt{\vec{v}^2} \simeq 270$ km/s) of the flow. We reanalyze the effect of the Sun’s gravity on the annual modulation of the WIMP signal in section V. Our results there are in qualitative agreement with those of Griest.

In summary, our purpose is to study the effect of Sun’s gravity on a flow of collisionless dark matter in the limit of zero velocity dispersion. The effect of finite velocity dispersion can be taken account by integrating over a distribution of initial velocities. The results can be applied to the flows, or streams, predicted by any specific halo model.

This paper is organized as follows. In section II, we give a general discussion of cold (i.e., zero velocity dispersion) flows and associated caustics. We derive formulas for the density of such flows that will be useful in subsequent sections. In section III, we derive the density and velocity distributions of a stationary cold dark matter flow past a point mass. In that case, all the results are analytical and exact. In section IV, we derive the density and velocity distributions of a stationary cold dark matter flow past a spherically symmetric mass distribution like that of our Sun. In this case, the trajectories that go through the Sun are calculated numerically. The skirt caustic phenomenon appears here. In section V, we extend our formalism to dark matter velocities with arbitrary velocity distribution, and apply the results to the isothermal model as an example. In section VI, we summarize our findings.

II. DENSITY FORMULAS

Here we derive expressions for the physical space density of a flow with zero velocity dispersion, using the general approach of ref. [12]. In such a flow each particle carries a 3-dimensional label $\vec{\alpha} = (\alpha_1, \alpha_2, \alpha_3)$. The flow is entirely defined by giving the positions $\vec{x}(\vec{\alpha}, t)$ of all particles at all times. The velocity of particle $\vec{\alpha}$ is $\vec{v}(\vec{\alpha}, t) = \partial \vec{x}(\vec{\alpha}, t) / \partial t$. In general, the map $\vec{\alpha} \rightarrow \vec{x}$ is one to many. Hence, at each point \vec{r} of space, there is a discrete set of flows with velocities $\vec{v}_j(\vec{r}, t) = \vec{v}(\vec{\alpha}_j(\vec{r}, t), t)$, $j = 1 \dots n(\vec{r}, t)$, where $\vec{\alpha}_j(\vec{r}, t)$ are the solutions of $\vec{r} = \vec{x}(\vec{\alpha}, t)$. $n(\vec{r}, t)$ is the number of distinct flows at (\vec{r}, t) . The total number of particles is

$$N = \int d^3\alpha \frac{d^3N}{d\alpha_1 d\alpha_2 d\alpha_3}(\vec{\alpha}) = \int d^3r \sum_{j=1}^n \frac{d^3N}{d\alpha_1 d\alpha_2 d\alpha_3} \frac{1}{|\det\left(\frac{\partial\vec{x}}{\partial\vec{\alpha}}\right)|} \Big|_{\vec{\alpha}=\vec{\alpha}_j(\vec{r},t)}. \quad (2.1)$$

The density of particles in physical space is therefore:

$$d(\vec{r}, t) = \sum_{j=1}^n \frac{d^3N}{d\alpha_1 d\alpha_2 d\alpha_3}(\vec{\alpha}_j(\vec{r}, t)) \frac{1}{|D(\vec{\alpha}_j(\vec{r}, t), t)|}, \quad (2.2)$$

where

$$D(\vec{\alpha}, t) \equiv \det\left(\frac{\partial\vec{x}}{\partial\vec{\alpha}}\right). \quad (2.3)$$

The formula for the density is manifestly $\vec{\alpha} \rightarrow \vec{\beta}(\vec{\alpha})$ reparametrization invariant.

The number of flows $n(\vec{r}, t)$ can change from point to point. Wherever a change occurs, n changes necessarily by two, i.e. two flows are added or two flows disappear. At those places the map $\vec{\alpha} \rightarrow \vec{x}$ is singular, D vanishes and the density d is infinite. Such places are called caustics. Caustics are generically surfaces because the condition $D = 0$ defines a surface. Only in degenerate cases are caustics lines or points.

A convenient generic parametrization of a zero velocity dispersion flow is as follows. Choose a surface \mathcal{S} that each particle crosses at least once in the course of its trajectory. \mathcal{S} may be time-dependent. Let $\vec{\alpha} = (\alpha_1, \alpha_2, t_0)$ where t_0 is the time the particle crosses \mathcal{S} for the first time, and (α_1, α_2) labels the crossing point on \mathcal{S} . Then

$$\frac{d^3N}{d\alpha^3} = \frac{d^3N}{d\alpha_1 d\alpha_2 dt_0} = F(\alpha_1, \alpha_2, t_0) \frac{d^2\mathcal{S}}{d\alpha_1 d\alpha_2}(\alpha_1, \alpha_2, t_0) \quad (2.4)$$

where $F(\alpha_1, \alpha_2, t_0)$ is the flux of particles through the surface. For a stationary flow it is natural to choose a time-independent surface \mathcal{S} , and a time-independent parametrization (α_1, α_2) of the points on \mathcal{S} . F and $\frac{d^2\mathcal{S}}{d\alpha_1 d\alpha_2}$ are t_0 -independent then, and $\vec{x}(\alpha_1, \alpha_2, t_0; t) = \vec{x}(\alpha_1, \alpha_2, t - t_0)$.

In the case of a flow which is initially uniform in space, with density $d_\infty(t_0)$ and velocity $\vec{v}_\infty = v_\infty(t_0)\hat{z}$, and which is incident upon a spherically symmetric mass distribution, the flow is axially symmetric about \hat{z} . It is natural to choose for \mathcal{S} a plane perpendicular to \hat{z} at large negative z and $(\alpha_1, \alpha_2) = (b, \varphi)$ where b is the impact parameter and φ is the azimuthal angle about the \hat{z} -axis. In this case:

$$\vec{x}(b, \varphi, t_0; t) = (\hat{x} \cos \varphi + \hat{y} \sin \varphi) \rho(b, t_0; t) + \hat{z} z(b, t_0; t) \quad (2.5)$$

provided we adopt the convention that ρ can be negative as well as positive and restrict $0 \leq \varphi \leq \pi$. We also let b have either sign. [In the usual cylindrical coordinates, where $\rho \geq 0$ and $0 \leq \varphi \leq 2\pi$, Eq. (2.5) would be invalid because φ changes by π when the z -axis is crossed.] From Eq. (2.5) follows:

$$\det\left(\frac{\partial\vec{x}}{\partial\vec{\alpha}}\right) = \rho \det\left(\frac{\partial(\rho, z)}{\partial(b, t_0)}\right). \quad (2.6)$$

Moreover

$$\frac{d^3 N}{d\alpha^3} = F(t_0) \frac{d^2 \mathcal{S}}{db d\varphi} = d_\infty(t_0) v_\infty(t_0) |b| \quad . \quad (2.7)$$

Hence, Eq. (2.2) becomes

$$d(\rho, z) = \frac{1}{|\rho|} \sum_{j=1}^n \frac{|b| d_\infty(t_0) v_\infty(t_0)}{\left| \det \left(\frac{\partial(\rho, z)}{\partial(b, t_0)} \right) \right|} \Big|_{b=b_j(\rho, z, t), t=t_{0j}(\rho, z, t)} \quad (2.8)$$

where $b_j(\rho, z, t)$ and $t_{0j}(\rho, z, t)$ are the solutions of $\rho(b, t_0; t) = \rho$, $z(b, t_0; t) = z$. If the flow is stationary, d_∞ and v_∞ are t_0 -independent, $\rho(b, t_0; t) = \rho(b, t-t_0)$, and $z(b, t_0; t) = z(b, t-t_0)$. In that case

$$d(\rho, z) = \frac{d_\infty v_\infty}{|\rho|} \sum_{j=1}^n \frac{|b|}{\left| \det \left(\frac{\partial(\rho, z)}{\partial(b, t)} \right) \right|} \Big|_{b=b_j(\rho, z), t=t_j(\rho, z)} \quad (2.9)$$

where the t_j and b_j are the solutions of $\rho(b, t-t_0) = \rho$ and $z(b, t-t_0) = z$.

III. COLD FLOW PAST A POINT MASS

In this section we derive the density and velocity distribution of collisionless particles in a stationary zero velocity dispersion flow past a point mass M . The flow is axially symmetric as well as stationary. Let d_∞ and $\vec{v}_\infty = v_\infty \hat{z}$ be the uniform density and velocity in the absence of M , and (z, ρ, φ) cylindrical coordinates centered on the point mass. The trajectory of the particle with impact parameter b is given in parametric form by [32]:

$$\begin{aligned} t(b, \psi) &= \frac{a}{v_\infty} (e \sinh \psi - \psi) \\ z(b, \psi) &= a(e \sinh \psi + 1 - \frac{1}{e} \exp \psi) \\ \rho(b, \psi) &= b(1 - \frac{1}{e} \exp \psi), \end{aligned} \quad (3.1)$$

where $a \equiv \frac{GM}{v_\infty^2}$, ψ is the “eccentric anomaly” parameter, and $e \equiv \sqrt{1 + \left(\frac{b}{a} \right)^2}$. Fig. 1 illustrates a pair of trajectories. As in the previous section, we do not use cylindrical coordinates in the conventional way. We allow ρ to have either sign, but restrict φ to take values between 0 and π . Also we let b have either sign.

The velocity components of the flow are:

$$\begin{aligned} v_\rho &= \frac{\partial \rho}{\partial \psi} \frac{\partial \psi}{\partial t} = -v_\infty \frac{b \exp \psi}{e a (e \cosh \psi - 1)} \\ v_z &= \frac{\partial z}{\partial \psi} \frac{\partial \psi}{\partial t} = v_\infty \frac{e \cosh \psi - \frac{1}{e} \exp \psi}{e \cosh \psi - 1} \quad . \end{aligned} \quad (3.2)$$

The density distribution is given by Eq. (2.9). In the point mass case, $n = 2$ everywhere. Upon changing variables $t \rightarrow \psi$, we obtain:

$$\begin{aligned}
d(\rho, z) &= \frac{d_\infty v_\infty}{|\rho|} \sum_{j=1}^2 \frac{|b| \left| \frac{dt}{d\psi} \right|}{\left| \det \left(\frac{\partial(\rho, z)}{\partial(b, \psi)} \right) \right|} \Big|_{b=b_j(\rho, z), \psi=\psi_j(\rho, z)} \\
&= d_\infty a \sum_{j=1}^2 \frac{(e \cosh \psi - 1)}{(1 - \frac{1}{e} \exp \psi) |D_2(b, \psi)|} \Big|_{b=b_j(\rho, z), \psi=\psi_j(\rho, z)}
\end{aligned} \tag{3.3}$$

where $b_j(\rho, z)$ and $\psi_j(\rho, z)$ are the two solutions of $\rho(b, \psi) = \rho$ and $z(b, \psi) = z$, and

$$\begin{aligned}
D_2(b, \psi) &\equiv \det \left(\frac{\partial(\rho, z)}{\partial(b, \psi)} \right) \\
&= \frac{a}{2} \left(e \exp(-\psi) - 1 + \left(e - \frac{2}{e} \right) \exp \psi + \exp(2\psi) \right).
\end{aligned} \tag{3.4}$$

Eqs. (3.1) can be inverted:

$$\begin{aligned}
b_\pm(\rho, z) &= \frac{\rho}{2} \left(1 \pm \sqrt{1 + y} \right) \\
\psi_\pm(\rho, z) &= \ln \left[e_\pm \frac{1}{y} \left(1 \mp \sqrt{1 + y} \right)^2 \right]
\end{aligned} \tag{3.5}$$

where $e_\pm = \sqrt{1 + (\frac{b_\pm}{a})^2}$ and

$$y \equiv \frac{4a}{\rho^2} (r + z) = \frac{2a}{r \sin^2(\theta/2)} , \tag{3.6}$$

with $r = \sqrt{\rho^2 + z^2}$ and $\theta = \tan^{-1}(\rho/z)$. Henceforth we label the two flows with $j = \pm$. Inserting Eqs. (3.5) into Eqs. (3.4) and (3.3) yields:

$$D_{2\pm} = r \frac{2 \sqrt{1 + y}}{\sqrt{1 + y} \pm 1} \tag{3.7}$$

and

$$d_\pm = \frac{d_\infty}{4} \left(\sqrt{1 + y} + \frac{1}{\sqrt{1 + y}} \pm 2 \right). \tag{3.8}$$

Note that $d_+ - d_- = d_\infty$ everywhere. The velocities are:

$$\begin{aligned}
v_{\rho\pm} &= -\frac{v_\infty}{r} (b_\pm - \rho) \\
v_{z\pm} &= v_\infty \left(1 + \frac{a \rho}{r b_\pm} \right) .
\end{aligned} \tag{3.9}$$

The total density

$$d = d_+ + d_- = \frac{d_\infty}{2} \left(\sqrt{1 + \frac{2a}{r \sin^2(\theta/2)}} + \frac{1}{\sqrt{1 + \frac{2a}{r \sin^2(\theta/2)}}} \right) . \tag{3.10}$$

It diverges on the positive \hat{z} -axis as

$$d \simeq d_\infty \frac{\sqrt{2a}z}{|\rho|} \quad . \quad (3.11)$$

This divergence occurs because the flow is focussed onto the positive \hat{z} -axis by the point mass' gravity. Each trajectory crosses the positive \hat{z} -axis, at $z = \frac{b^2}{2a}$. The positive \hat{z} -axis is the location of a line caustic, which we call the 'spike'. Eq. (3.11) is valid also for a finite size but spherically symmetric mass, at z large enough that the trajectories there did not pass through the mass.

As we remarked already in section II, caustics are generally surfaces rather than lines or points [12]. A line or point caustic is a degenerate case. The caustic of Eq. (3.11) is a line only because of the axial symmetry of the flow. If less symmetry is present - e.g. if the mass has a quadrupole moment, or if the initial velocity field of the flow is inhomogeneous - there is still a caustic downstream of the mass but it is a surface. Since it can collapse to a line, the surface is a tube of some sort. The structure of the tube is a problem left for future investigations.

IV. COLD FLOW PAST A SPHERICALLY SYMMETRIC MASS

In this section we derive the density and velocity distribution of a zero velocity dispersion flow past a spherically symmetric mass distribution of total mass M_\odot . The mass distribution is characterized by a radius R_\odot outside of which the density rapidly approaches zero. The trajectories passing through the mass must be calculated numerically. As before, the only force acting is the gravity of M_\odot . The density d_∞ and velocity $\vec{v}_\infty = v_\infty \hat{z}$ of the flow long before encountering the mass distribution are assumed to be constant in both space and time. Axial symmetry is preserved and the flow is stationary.

The density and velocity distributions derived in the previous section (III) are valid here provided the trajectories did not pass through the mass distribution at any point in their past. Defining b_\odot to be the impact parameter of the trajectory grazing the surface of the mass distribution, all results of the point mass case hold for trajectories labeled by $b > b_\odot$. The $b > b_\odot$ trajectories are given in parametric form by Eqs. (3.1) which implies $r = a(e \cosh \psi - 1)$. The point of closest approach to the mass is where $\psi = 0$. Setting $\psi = 0$ and $r = R_\odot$ gives the grazing impact parameter

$$b_\odot = R_\odot \sqrt{1 + 2a/R_\odot} \quad . \quad (4.1)$$

On the other hand, all trajectories for $b < b_\odot$ will pass through the mass distribution at some point in their motion.

Here it is convenient to work in spherical coordinates (r, θ, φ) . As in the previous section the azimuth φ is restricted to be between 0 and π . We measure the polar angle θ from the $+\hat{z}$ -direction and it takes values between $-\pi$ and $+\pi$. In this system of coordinates the polar angle smoothly changes sign as a trajectory crosses the symmetry axis downstream from the mass. As before, we let b have either sign.

We derive the density distribution of a stationary flow with axial symmetry in spherical coordinates. Analogously to Eqs. (2.6) and (2.9), we have

$$\det \left(\frac{\partial \vec{x}}{\partial \vec{\alpha}} \right) = r^2 \sin \theta \det \left(\frac{\partial(r, \theta)}{\partial(b, t_0)} \right) \quad (4.2)$$

and

$$d(r, \theta) = \frac{d_\infty v_\infty}{r^2 |\sin \theta|} \sum_{j=1}^n \frac{|b|}{\left| \det \left(\frac{\partial(r, \theta)}{\partial(b, t)} \right) \right|} \Big|_{b=b_j(r, \theta), t=t_j(r, \theta)} . \quad (4.3)$$

The index j counts the flows. In the point mass case, particles with impact parameter close to zero are scattered by an angle close to 180° . In that case, $n = 2$ everywhere. On the other hand, if the mass has finite size, there is a maximum scattering angle $|\Theta_{\max}| < 180^\circ$. This angle defines a cone. Far from the mass, $n = 1$ for $|\theta| > |\Theta_{\max}|$ whereas $n = 3$ for $|\theta| < |\Theta_{\max}|$. Since the number of flows changes on the surface of the cone, we expect a caustic there.

We break the sum over j into two parts. The first sum is over the flows for which we have calculated an exact result: the $b > b_\odot$ flows at any time in their motion and the $b < b_\odot$ flows before entering the mass distribution. We label these flows by the index k ($= 1, \dots, n_k$). The second sum is over the flows which must be calculated numerically, namely the $b < b_\odot$ flows at any time after they have entered the mass distribution. We label these flows by the index l ($= 1, \dots, n_l$). The density is then

$$d(r, \theta) = \sum_{k=1}^{n_k} d_k(r, \theta) + \frac{d_\infty v_\infty}{r^2 |\sin \theta|} \sum_{l=1}^{n_l} \frac{|b|}{\left| \det \left(\frac{\partial(r, \theta)}{\partial(b, t)} \right) \right|} \Big|_{b=b_l(r, \theta), t=t_l(r, \theta)} \quad (4.4)$$

where the $d_k(r, \theta)$ expressions were derived in section III and the terms in the sum over l we address next. Although we have not shown it explicitly Eq. (4.4), n_k and n_l are dependent upon (r, θ) . We will see that $(n_k, n_l) = (1, 0), (1, 2), (2, 1), (0, 1)$ or $(0, 3)$, depending on position.

To simplify the determinant, while exposing the caustic features intrinsic to Eq. (4.4), we take the limit where $r \gg R_\odot, a$. In that case, for the l -flows

$$\det \left(\frac{\partial(r, \theta)}{\partial(b, t)} \right) \simeq v_\infty \frac{\partial \theta}{\partial b} . \quad (4.5)$$

Hence

$$d_l(r, \theta) \simeq \frac{d_\infty}{r^2 |\sin \theta|} \frac{|b_l|}{\left| \frac{d\theta}{db_l} \right|} \quad (4.6)$$

and the numerical computation of the second term in Eq. (4.4) becomes straightforward. For the l -flows at $r \gg R_\odot$ and a , $|\theta(b)|$ is the scattering angle for the trajectory of impact parameter $|b|$. The scattering angle of a particle incident at impact parameter b with initial kinetic energy E upon a central potential $V(u)$ is [32]

$$\Theta(|b|) = \pi - 2 \int_0^{u_{\max}} \frac{|b| du}{\sqrt{1 - V(u)/E - b^2 u^2}} , \quad (4.7)$$

where $u \equiv 1/r$ and $u_{\max} = 1/r_{\min}$. We express the potential as $V(x) = GM_{\odot}\phi(x)/R_{\odot}$ with $x \equiv r/R_{\odot}$. We choose the potential of the mass distribution to be

$$\phi(x) = - \left[\frac{\alpha + \beta x^6}{1 + \gamma x^2 + \beta x^7} \right], \quad (4.8)$$

setting $\alpha = 5$, $\beta = 5000$, and $\gamma = 8$ to give a close fit to the solar mass distribution [33]. Thus, all of the following calculations should be considered relevant to the Sun. In Eq. (4.8), $\phi \simeq -1/x$ for $x > 1$, the point mass limit, and $\phi \simeq -\alpha + \gamma x^2$ for $x \ll 1$ reflecting the fact that the density in the solar core is constant. The potential (4.8) is plotted in Fig. 2 in comparison to $\phi = -1/x$.

We calculate the scattering angle $\Theta(|b|)$ for the potential of Eq. (4.8). For comparison, the scattering angle for the $\phi = -1/x$ potential is the exact result

$$\Theta(b) = - 2 \arcsin \left(\frac{1}{e} \right) \text{sign}(b), \quad (4.9)$$

in which $\Theta(b)$ can take values between $-\pi$ and $+\pi$. We plot $\Theta(b)$ for the distributed mass and point mass cases in Fig. 3 calculated for two flow velocities, $v_{\infty} = 200$ km/sec and 500 km/sec.

In Fig. 3 there is a maximum scattering angle $\Theta_{\max} < \pi$. For $0 < \theta < \Theta_{\max}$, there are two flows labeled by different values of b with $\text{sign}(b) = -\text{sign}(\theta)$. In addition, there is a flow for which b and θ have the same sign. For large r , the third flow is in the sum over k . In the notation of section III, it has impact parameter b_+ . So $n = 3$, for large r and $|\theta| < \Theta_{\max}$. For $\Theta_{\max} < |\theta| < \pi$, the two flows of Fig. 3 are absent but the b_+ flow is still present, so $n = 1$ there.

Near the cone $|\theta| = \Theta_{\max}$ is a caustic surface which we call the “skirt.” The determinant in Eq. (4.4) vanishes there since $d\theta/db = 0$. We calculated the maximum scattering angle Θ_{\max} as a function of flow velocity v_{∞} ranging from 100 km/sec to 1000 km/sec. See Fig. 4 for the result.

We now examine the density Eq. (4.4) near the skirt caustic for angles $\theta < \Theta_{\max}$. The function $\Theta(b)$ can be approximated near Θ_{\max} as

$$\Theta(b) \simeq \Theta_{\max} - \frac{1}{2}H(b - b_c)^2 \quad (4.10)$$

where b_c is the impact parameter for the maximum scattering angle, and $H \equiv -\frac{d^2\Theta}{db^2}|_{b=b_c}$. For θ near to but smaller than Θ_{\max} , we have $n_k = 1$ and $n_l = 2$ in Eq. (4.4). The $k = 1$ flow is the one labeled + in section III. Using Eqs. (4.5) and (4.10), we get the approximate density near the skirt

$$d_{\text{skirt}} \simeq d_+ + \frac{d_{\infty} b_c}{r^2 \sin \Theta_{\max}} \sqrt{\frac{2}{H(\Theta_{\max} - \theta)}} \quad \text{for } \theta < \Theta_{\max} \quad (4.11)$$

$$= d_+ \quad \text{for } \theta > \Theta_{\max}. \quad (4.12)$$

A generic feature of caustic surfaces is evident in Eq. (4.12), namely that the density diverges near the surface as $1/\sqrt{\Theta_{\max} - \theta}$ when the skirt is approached from $\theta < \Theta_{\max}$ side. The density remains constant (equal to d_+) when the surface is approached from $\theta > \Theta_{\max}$.

The strength of the caustic is proportional to $b_c/r^2 \sin \Theta_{\max} \sqrt{H}$. We plot H and b_c over a range of flow velocities in Figs. 5 and 6, respectively. For comparison, we plot b_c alongside the grazing impact parameter b_\odot .

Moving away from the skirt toward smaller values of $|\theta|$, an angle Θ_\odot will be reached where the flows change from $n_k = 1, n_l = 2$ to $n_k = 2, n_l = 1$. $\Theta_\odot = \Theta(b_\odot)$ is the scattering angle of the grazing trajectories. Using Eq. (4.1) gives

$$\Theta_\odot = -2 \arcsin \left(\frac{a}{a + R_\odot} \right) \operatorname{sign}(b_\odot). \quad (4.13)$$

For $|\theta| < |\Theta_\odot|$, only one flow passed through the solar interior. We plot Θ_\odot in Fig. 4 as a function of the flow velocity v_∞ .

For $r \gg R_\odot$ and a ,

$$\begin{aligned} (n_k, n_l) &= (1, 0) & \text{for } |\theta| > |\Theta_{\max}| \\ &= (1, 2) & \text{for } |\Theta_\odot| < |\theta| < |\Theta_{\max}| \\ &= (2, 1) & \text{for } |\theta| < |\Theta_\odot|. \end{aligned} \quad (4.14)$$

There are two regions in or near the Sun where different (n_k, n_l) values arise. First, $(n_k, n_l) = (0, 1)$ on the interior of the Sun on the upstream side. Second, there is a region near the Sun on the downstream side where $(n_k, n_l) = (0, 3)$. The flow properties in these regions are calculable with Eq. (4.4). We leave that task for future investigations.

The velocity distributions for the k -flows are given in Eq. (3.9). For the l -flows, using energy and angular momentum conservation,

$$\begin{aligned} v_{r_l} &= v_\infty \sqrt{1 + \frac{2a}{r} - \left(\frac{b_l}{r} \right)^2}, \\ v_{\theta_l} &= v_\infty \frac{b_l}{r}. \end{aligned} \quad (4.15)$$

For the l -flows at large r , θ is the scattering angle Θ . Hence, the $b_l(\theta)$ are given by Fig. 3.

Using $\Theta(b)$ it is straight-forward to calculate the full expression for the density distribution at large r including the flows through the Sun. This result is given in Fig. 7 for the mean Earth–Sun distance. The density field of a $b < b_\odot$ flow, at large r , is smaller than the sum of the $b > b_\odot$ flows, roughly by the factor $\frac{b_\odot^2}{r^2}$. Away from the caustic skirt, the flows through the Sun contribute only 4×10^{-3} to 4×10^{-5} of the total density at the Earth’s location for velocities ranging from $v_\infty = 100$ km/sec to 1000 km/sec.

The limit $R_\odot \rightarrow 0$ seems paradoxical. In section III we found that $n = 2$ everywhere, whereas here $n = 1$ for $|\theta| > |\Theta_{\max}|$ and $n = 3$ for $|\theta| < |\Theta_{\max}|$. What happens is that when $R_\odot \rightarrow 0$ and $\Theta_{\max} \rightarrow \pi$ one of the three flows acquires vanishing density. The flow that disappears is the one with the smallest impact parameter for given scattering angle in Fig. 3. The flows that survive are the flow with the largest impact parameter for given scattering angle in Fig. 3 and the flow with $\operatorname{sign}(\theta) = \operatorname{sign}(b)$, i.e., the flow labeled + in section III.

To conclude this section, we briefly discuss the relationship between the density distribution formulas for a flow past a point mass and the Rutherford differential cross-section formula. The differential scattering cross-section is

$$\frac{d\sigma}{d\Omega}(\theta) = \frac{b}{\sin \theta} \left| \frac{db}{d\theta} \right|, \quad (4.16)$$

and the Rutherford formula for scattering in a r^{-1} potential is

$$\frac{d\sigma}{d\Omega}(\theta)_R = \frac{a^2}{4 \sin^4(\theta/2)}, \quad (4.17)$$

where $a \equiv GM/v_\infty^2$ as before. Consider only the “ $-$ flow,” in the notation of section III, in the limit where $r \gg a$ and $\theta \neq 0$. As shown above, the determinant then simplifies, $\left| \det \left(\frac{\partial(r,\theta)}{\partial(b,t)} \right) \right| \rightarrow v_\infty \left| \frac{db}{d\theta} \right|$, and the density can be written in terms of the Rutherford formula Eq. (4.17):

$$d_-(r, \theta) = \frac{d_\infty}{r^2} \frac{b}{\sin \theta} \left| \frac{db}{d\theta} \right| = \frac{d_\infty}{r^2} \frac{d\sigma}{d\Omega}(\theta)_R. \quad (4.18)$$

Using a fact derived in section III, namely that $d_+ - d_- = d_\infty$ everywhere, we get

$$d_+(r, \theta) = d_\infty \left(1 + \frac{a^2}{4r^2 \sin^4(\theta/2)} \right). \quad (4.19)$$

One can verify that the Eqs. (4.18) and (4.19) agree with the exact results for d_\pm derived in section III. Taking the $r \rightarrow \infty$ limit of Eq. (3.8) at fixed $\theta \neq 0$ and keeping the terms to leading order yields Eqs. (4.18) and (4.19).

V. HOT FLOW PAST A POINT MASS

In many discussions of dark matter detection on Earth, it is assumed that the distribution in the galactic halo is isothermal. The local velocity distribution is then

$$f(\vec{v}_\infty) = \frac{d_\infty}{(\sqrt{\pi}\sigma)^3} \exp\left[-\frac{1}{\sigma^2}(\vec{v}_\infty + \vec{v}_\odot)^2\right] \quad (5.1)$$

in the absence of the Sun, for an observer moving with the Sun’s velocity \vec{v}_\odot . $\sigma = \sqrt{\frac{2}{3} \langle v^2 \rangle} \simeq 220$ km/s, where $\langle v^2 \rangle^{1/2}$ is the velocity dispersion of the galactic halo. σ and v_\odot are approximately equal. As was mentioned in the Introduction, there is little theoretical motivation for assuming an isothermal distribution. Indeed most of our paper is concerned with discrete flows, which we believe to be the relevant description. However our methods can also be applied to smooth velocity distributions such as Eq. (5.1). This is done in this section. We neglect here the Sun’s size, treating it as a point mass.

If the velocity distribution in the absence of the Sun is $f(\vec{v}_\infty)$ independently of position, what is the position-dependent velocity distribution $f_\odot(\vec{r}, \vec{v})$ when the effect of the Sun’s gravity is included? The answer to this seemingly daunting question is [22,20]:

$$f_\odot(\vec{r}, \vec{v}) = f(\vec{v}_\infty(\vec{r}, \vec{v})) \quad (5.2)$$

where $\vec{v}_\infty(\vec{r}, \vec{v})$ is the initial velocity of the trajectory that passes by position \vec{r} with velocity \vec{v} . Indeed, Liouville’s theorem states that phase-space density is conserved along particle

trajectories. Since $f(\vec{v}_\infty)$ is the initial phase-space density, when the particles are far from the Sun, and $f_\odot(\vec{r}, \vec{v})$ is the final phase-space density, Eq. (5.2) follows.

To obtain $\vec{v}_\infty(\vec{r}, \vec{v})$, we exploit the constants of the motion:

$$\begin{aligned} E &= \frac{1}{2}v^2 - \frac{GM_\odot}{r} \\ \vec{l} &= \vec{r} \times \vec{v} \\ \vec{A} &= \vec{v} \times (\vec{r} \times \vec{v}) - GM_\odot \hat{r} \quad . \end{aligned} \quad (5.3)$$

E , \vec{l} , and \vec{A} are the energy, angular momentum and Laplace–Runge–Lenz vector, per unit mass in each case. In the initial state,

$$\begin{aligned} E &= \frac{1}{2}v_\infty^2 \\ \vec{l} &= -bv_\infty \hat{\varphi} \\ \vec{A} &= bv_\infty^2 \hat{\rho} + GM_\odot \hat{z}. \end{aligned} \quad (5.4)$$

where b is the impact parameter, \hat{z} is in the direction of the initial velocity ($\vec{v}_\infty = v_\infty \hat{z}$), $\hat{\varphi}$ is perpendicular to the plane of the trajectory and $\hat{\rho} = \hat{\varphi} \times \hat{z}$. The notation is consistent with that of section III. Since

$$v_\infty = +\sqrt{v^2 - \frac{2GM_\odot}{r}}, \quad (5.5)$$

it only remains to express \hat{z} in terms of \vec{r} and \vec{v} . We have:

$$\vec{A} \times \vec{l} = +bv_\infty^3 (a\hat{\rho} - b\hat{z}) \quad (5.6)$$

where $a = \frac{GM_\odot}{v_\infty^2}$, as before. Hence

$$\hat{z} = \frac{1}{(a^2 + b^2)v_\infty^2} (a\vec{A} - \frac{1}{v_\infty} \vec{A} \times \vec{l}) \quad . \quad (5.7)$$

Substituting Eqs. (5.3) into Eq. (5.7), we obtain after some algebra:

$$\vec{v}_\infty(\vec{r}, \vec{v}) = \frac{1}{a^2 v_\infty^2 + l^2} \left\{ \vec{v} \left[l^2 - av_\infty^2 r - av_\infty(\vec{r} \cdot \vec{v}) \right] + \vec{r} a v_\infty^2 \left[\frac{1}{r}(\vec{r} \cdot \vec{v}) + \frac{v^2}{v_\infty} - \frac{av_\infty}{r} \right] \right\} \quad (5.8)$$

where $l^2 = r^2 v^2 - (\vec{r} \cdot \vec{v})^2$ and v_∞ is given in terms of \vec{r} and \vec{v} by Eq. (5.5).

If the isothermal velocity distribution (5.1) is assumed, we have therefore:

$$f_\odot(\vec{r}, \vec{v}) = \frac{d_\infty}{(\sqrt{\pi}\sigma)^3} \exp\left[-\frac{1}{\sigma^2} v_G^2(\vec{r}, \vec{v})\right] \Theta(v_\infty^2(\vec{r}, \vec{v})) \quad (5.9)$$

where $\Theta(x) = 0$ for $x < 0$, 1 for $x > 0$, and

$$\begin{aligned} v_G^2(\vec{r}, \vec{v}) &= (\vec{v}_\odot + \vec{v}_\infty(\vec{r}, \vec{v}))^2 = \vec{v}_\odot^2 + \vec{v}_\infty^2 + 2v_\odot \frac{1}{a^2 v_\infty^2 + l^2} \cdot \\ &\quad \cdot \left\{ v \cos \alpha \left[l^2 - av_\infty^2 r - av_\infty(\vec{r} \cdot \vec{v}) \right] + av_\infty^2 \cos \beta \left[\vec{r} \cdot \vec{v} + \frac{v^2 r}{v_\infty} - av_\infty \right] \right\} \quad , \end{aligned} \quad (5.10)$$

where α is the angle between \vec{v}_\odot and the dark matter velocity \vec{v} and β is the angle between \vec{v}_\odot and the position \vec{r} of the observer relative to the Sun. A formula for $v_G^2(\vec{r}, \vec{v})$ was obtained by J.M.A. Danby and G.L. Camm [22] over 40 years ago. K. Griest [20] obtained a formula which differs from that of Danby and Camm. Our formula appears different from both that of Danby and Camm, and that of Griest. We verified that the RHS of Eq. (5.8) is indeed v_∞^2 , and that Eq. (5.8) checks out in the $l = 0$ and $l \rightarrow \infty$ limits, in the $a = 0$ limit, and when $\vec{v}_\infty \parallel \vec{r}$.

The annual modulation of the event rate in WIMP dark matter searches is caused for the most part by the seasonal variation of the flux of dark matter particles as the Earth's orbital motion adds to or subtracts from the motion of the Sun through the galactic halo. As was discussed in the Introduction, there is an additional contribution because the Sun's gravity modifies the density and velocity distributions in the solar neighborhood. The combined effects of the Earth's orbital motion and the Sun's gravity can be computed if we know the distribution of dark matter in the Earth's frame of reference. Following Griest, that is obtained by simply replacing \vec{v}_\odot in Eqs. (5.9) and (5.10) by $\vec{v}_\odot + \vec{v}_\oplus$ where \vec{v}_\oplus is the velocity of the Earth relative to the Sun. The event rate depends also on the WIMP mass and such experimental variables as the detector threshold, the target mass and, of course, the scattering cross-section.

The effect of the Sun's gravity on the event rate in WIMP searches is largely due to the change in the density of dark matter. Moreover the signal from axion to photon conversion in the cavity detector of galactic halo axions is simply proportional to the dark matter density. So let us calculate the density $d(r, \theta)$ where r is the distance to the Sun and θ is the angle between \vec{r} and \vec{v}_\odot . We could integrate Eq. (5.9) over \vec{v} . However, it is easier to integrate

$$d(r, \theta) = \int d^3v_\infty f(\vec{v}_\infty) d(\vec{r}, \vec{v}_\infty) \quad (5.11)$$

where $d(\vec{r}, \vec{v}_\infty)$ is the density due to a single flow of initial velocity \vec{v}_∞ , Eq. (3.10). This yields

$$d(r, \theta) = \frac{d_\infty}{\pi^{\frac{3}{2}}} \int_0^\infty u^2 du \int_{-1}^{+1} ds \int_0^{2\pi} d\varphi \exp[-(u^2 + u_\odot^2 + 2uu_\odot s)] \cdot \frac{1}{2} \left(\sqrt{1 + \frac{4}{X}} + \frac{1}{\sqrt{1 + \frac{4}{X}}} \right) \quad (5.12)$$

where $u_\odot = \frac{v_\odot}{\sigma}$,

$$X = \frac{4}{y} = \frac{r}{a_\sigma} u^2 (1 - s \cos \theta - \sqrt{1 - s^2} \sin \theta \cos \varphi) \quad (5.13)$$

and $a_\sigma \equiv \frac{GM_\odot}{\sigma^2}$. The integral in Eq. (5.12) was evaluated numerically. Fig. 8 shows $d(r)$ in case the Sun were at rest with respect to the halo ($v_\odot = 0$). At the Earth's distance from the Sun, the density increase due to the Sun's gravity is approximately 3%.

Fig. 9 shows $d(r, \theta)$ as a function of θ for $v_\odot = \sigma = 220$ km/s and $r = 1.5 \times 10^{13}$ cm, the mean Earth-Sun distance. At the Earth's distance from the Sun, the density increase is approximately 0.5% upstream ($\theta = \pi$) and 6% downstream ($\theta = 0$). The large density

downstream is the spike caustic but spread out because of the large velocity dispersion. The Earth's orbit is inclined at approximately 60° relative to \vec{v}_\odot , with the Earth being most closely downstream of the Sun on March 3. Fig. 9 shows that the density variation between September 2 ($\theta = 120^\circ$) and March 3 ($\theta = 60^\circ$) is of order 1.4%. This is consistent with the earlier calculation of Griest [20].

VI. CONCLUSIONS

We analyzed the effect of the Sun's gravity on a flow of collisionless dark matter through the solar neighborhood. We were mainly concerned with the case of a cold flow, i.e. a flow with zero velocity dispersion. The cold flow results can be generalized to arbitrary flows by integrating over the initial \vec{v}_∞ velocity distribution. We neglected the effect of the Earth's gravity, but this is indeed small. The ratio of the Sun and Earth gravity effects is of order $\frac{M_\oplus}{R_\oplus} \frac{r}{M_\odot} \simeq 0.07$ where M_\oplus is the Earth's mass, R_\oplus its radius, and r is the mean Earth–Sun distance.

In section II, we obtained formulas for the density and velocity distributions of cold flows with axial symmetry. In section III, these formulas were applied to a cold uniform flow past a point mass. In that case the number of flows $n = 2$ everywhere. There is a caustic line, which we called the 'spike', downstream of the Sun. It is located on the positive \hat{z} –axis where \hat{z} is the direction of the incoming flow ($\vec{v}_\infty = v_\infty \hat{z}$). The profile of the spike is given in Eq. (3.11). The densities of the two flows everywhere are given by Eqs. (3.8), the velocity distributions by Eqs. (3.9). These are exact results.

In section III, we took account of the Sun's finite radius. We assumed that the solar mass distribution is spherically symmetric. Many of the results derived in section III are still valid. In particular, the spike caustic remains and its profile is still given by Eq. (3.11) for z large enough that the trajectories there did not go through the Sun in the past. A new caustic appears which we called the 'skirt'. It is located near the cone of axis \hat{z} and opening angle Θ_{\max} where Θ_{\max} is the maximum scattering angle. Inside this cone $n = 3$, whereas $n = 1$ outside the cone. The density enhancement associated with the skirt falls off as $\frac{1}{r^2}$ where r is the distance to the Sun, and is rather feeble on Earth even at the moment of skirt crossing. However, the profile of the density near the skirt depends on the mass distribution inside the Sun. In principle, by monitoring the densities of the various dark matter flows as we orbit the Sun, the mass distribution of the Sun can be investigated. The density profile near a skirt was obtained in terms of quantities H , b_c and Θ_{\max} , which we defined and computed as a function of v_∞ for a realistic model of the solar mass distribution.

In section IV, we applied our methods to the single flow of dark matter predicted by the isothermal model. That flow has direction $-\hat{\phi}_G$ opposite to the Sun's motion in the Galaxy and velocity dispersion $\sqrt{\vec{v}^2} \simeq 270$ km/s. We derived a formula which gives the velocity distribution at any point in the neighborhood of the Sun in terms of an arbitrary initial velocity distribution $f(\vec{v}_\infty)$. We also computed the density as a function of position relative to the Sun. There is a spike caustic downstream of the Sun but it is spread out because of the large velocity dispersion. In the isothermal model the density is largest (smallest) near March 3 (September 2). The amplitude of this density modulation is of order 0.7%.

VII. ACKNOWLEDGMENTS

P.S. would like to thank Doug Eardly for stimulating discussions on this topic several years ago. He is also grateful to the Aspen Center for Physics for its hospitality while working on this paper. This work was supported in part by the U.S. Department of Energy under grant DE-FG02-97ER41029.

REFERENCES

- [1] E.W. Kolb and M.S. Turner, *The Early Universe*, Addison-Wesley, 1990; M.Srednicki, Editor, *Particle Physics and Cosmology: Dark Matter*, North-Holland, 1990.
- [2] P. Sikivie, Phys. Rev. Lett. 51 (1983) 1415, and Phys. Rev. D32 (1985) 2988; C. Hagemann et al., Phys. Rev. Lett. 80 (1998) 2043; I. Ogawa, S. Matsuki and K. Yamamoto, Phys. Rev. D53 (1996) 1740.
- [3] M.W. Goodman and E. Witten, Phys. Rev. D31 (1985) 3059; I. Wasserman, Phys. Rev. D33 (1986) 2071; A. Drukier, K. Freese and D.N. Spergel, Phys. Rev. D33 (1986) 3495.
- [4] For reviews, see: J.R. Primack, D. Seckel and B. Sadoulet, Ann. Rev. Nucl. Part. Sci. 38 (1988) 751; P.F. Smith and J.D. Lewin, Phys. Rep. 187 (1990) 203; G. Jungman, M. Kamionkowski and K. Griest, Phys. Rep. 267 (1996) 195.
- [5] J. Silk, K. Olive and M. Srednicki, Phys. Rev. Lett. 55 (1985) 257; L.M. Krauss, K. Freese, D.N. Spergel and W.H. Press, Ap. J. 299 (1985) 1001.
- [6] A. Drukier, K. Freese and D. Spergel, Phys. Rev. D33 (1986) 3495; K. Freese, J. Frieman and A. Gould, Phys. Rev. D37 (1988) 3388.
- [7] J.N. Bahcall and R.M. Soneira, Ap. J. Suppl. 44 (1980) 73; J.A.R. Caldwell and J.P. Ostriker, Ap. J. 251, (1981) 61; M.S. Turner, Phys. Rev. D33 (1986) 889; R.A. Flores, Phys. Lett. B215 (1988) 73.
- [8] D. Lynden-Bell, Mon. Not. R. Astron. Soc. 136 (1967) 101.
- [9] P. Sikivie and J.R. Ipser, Phys. Lett. B291 (1992) 288.
- [10] P. Sikivie, Phys. Lett. B432 (1998) 139.
- [11] C. Hogan, astro-ph/9811290, to appear in Ap. J.; S. Tremaine, Mon. Not. R. Astron. Soc. 307 (1999) 877.
- [12] P. Sikivie, Phys. Rev. D60 (1999) 063501.
- [13] P. Sikivie, I. Tkachev and Y. Wang, Phys. Rev. Lett. 75 (1995) 2911, and Phys. Rev. D56 (1997) 1863.
- [14] P. Sikivie, in the Proceedings of the Second International Workshop on *The Identification of Dark Matter*, edited by N. Spooner and V. Kudryavtsev, World Scientific 1999, p.68, astro-ph/9810286.
- [15] W. Kinney and P. Sikivie, Phys. Rev. D61 (2000) 087305.
- [16] P. Sikivie, *Evidence for ring caustics in the Milky Way*, astro-ph/0109296.
- [17] J.A. Filmore and P. Goldreich, Ap. J. 281 (1984) 1; E. Bertschinger, Ap. J. Suppl. 58 (1985) 39.
- [18] J.F. Navarro, C.S. Frenk and S.D.M. White, Ap. J. 462 (1996) 563; B. Moore et al., Ap. J. Lett. 499 (1998) L5.
- [19] D. Stiff, L.M. Widrow and J. Frieman, Phys. Rev. D64 (2001) 083516.
- [20] K. Griest, Phys. Rev. D37 (1988) 2703.
- [21] H. Bondi and F. Hoyle, Mon. Not. R. Astron. Soc., 104 (1944) 273.
- [22] J.M.A. Danby and G.L. Camm, Mon. Not. R. Astron. Soc. 117 (1957) 50.
- [23] J.M.A. Danby and T.A. Bray, Astron. J. 72 (1967) 219.
- [24] For a discussion, see: C.J. Copi, J. Heo and L. Krauss, Phys. Lett. B461 (1999) 43.
- [25] J.D. Vergados, Phys. Rev. D63, (2001) 063511.
- [26] A.M. Green, Phys. Rev. D63 (2001) 103003.
- [27] G. Gelmini and P. Gondolo, Phys. Rev. D64 (2001) 023504.

- [28] P. Ullio and M. Kamionkowski, JHEP 0103 (2001) 049.
- [29] R. Bernabei et al., Phys. Lett. B450 (1999) 448, Phys. Lett. B480 (2000) 23.
- [30] R. Abusaidi et al., Phys. Rev. Lett. 84 (2000) 5699.
- [31] A. Benoit et al., Phys. Lett. B513 (2001) 15.
- [32] H. Goldstein, *Classical Mechanics*, Addison-Wesley, 1980.
- [33] C.W. Allen, *Astrophysical Quantities*, Athlone Press, London, 1976.

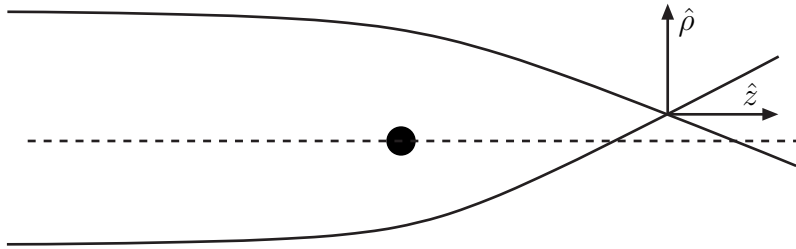


FIG. 1. Two trajectories past a spherically symmetric mass distribution. The incident flow is assumed to be uniform and to have vanishing velocity dispersion. If the scatterer is a point mass, the particles with small impact parameter are scattered by an angle close to 180° , and hence the number of flows $n = 2$ everywhere. If the scatterer is distributed over a finite radius, there is a maximum scattering angle $\Theta_{\max} < 180^\circ$. In that case, $n = 1$ upstream of the scatterer, and $n = 3$ downstream.

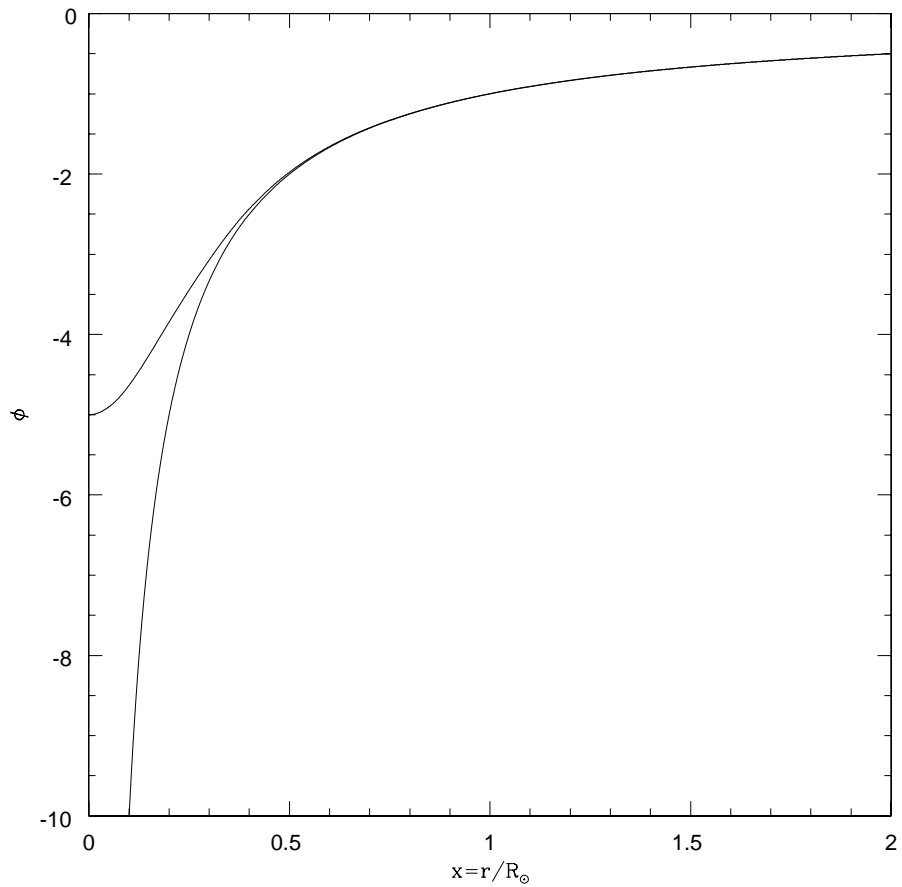


FIG. 2. A plot of the dimensionless Solar potential $\phi(x)$ given in Eq. (4.8) and compared with the point mass potential $\phi(x) = -1/x$.

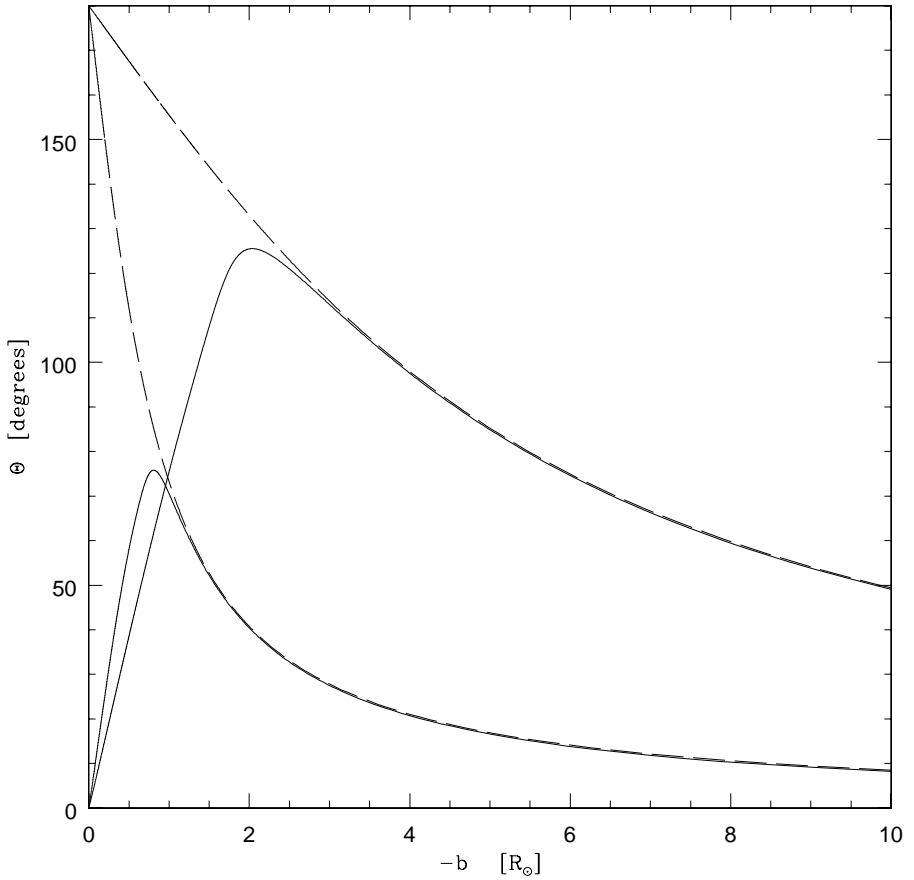


FIG. 3. The scattering angle for dark matter incident upon the Sun as a function of impact parameter, for flows of initial velocity 200 km/sec and 500 km/sec. The solid curves are for the distributed mass described in section IV and the dashed curves are for the point mass. The flows with lower initial velocities have larger scattering angle at large impact parameter.

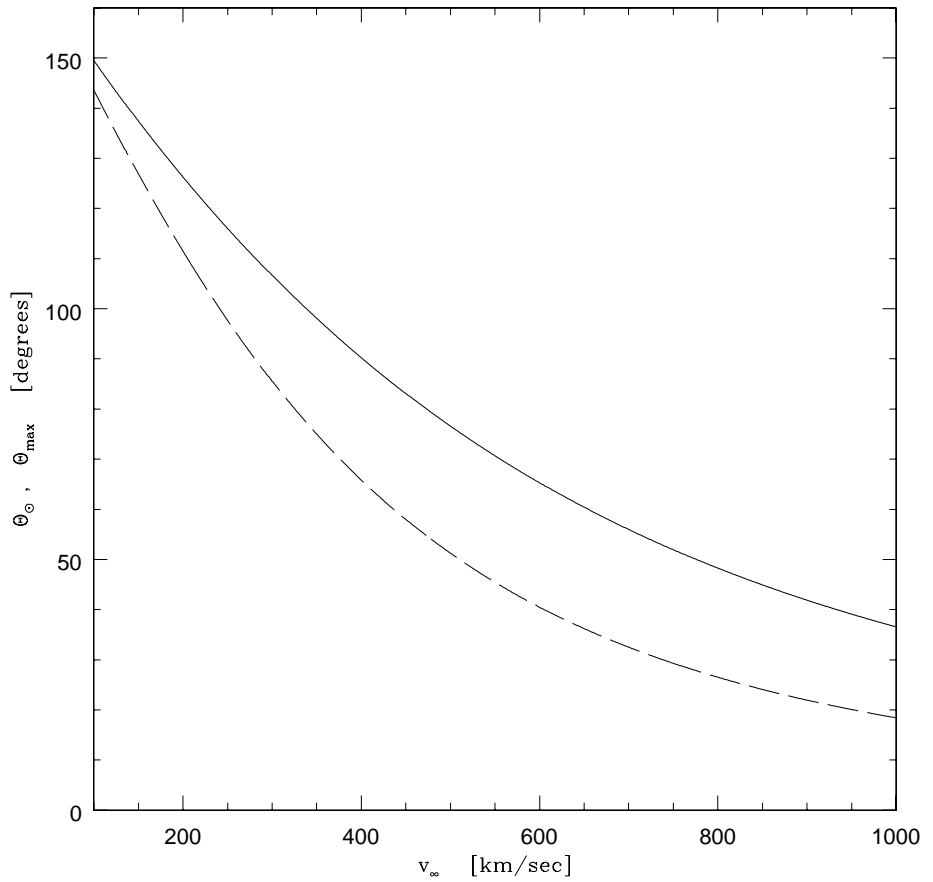


FIG. 4. The maximum scattering angle Θ_{\max} (solid line) and the scattering angle Θ_∞ of the grazing trajectory (dashed line) as a function of initial flow velocity v_∞ , for the solar model described in section IV.

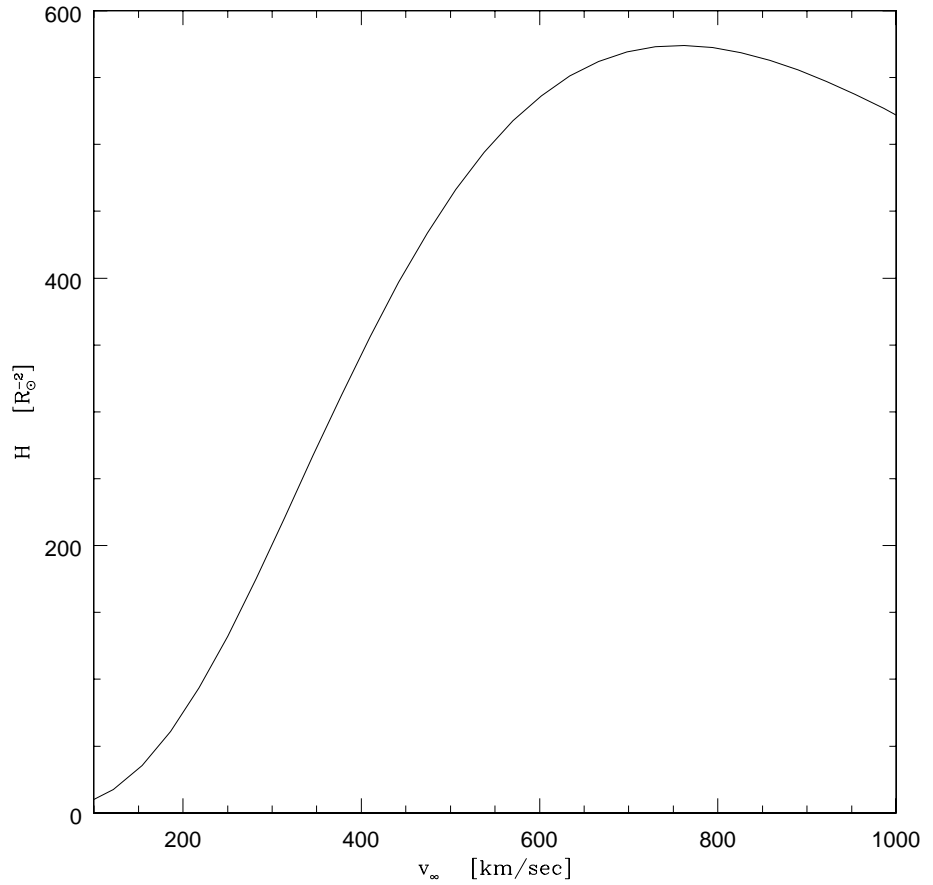


FIG. 5. The parameter $H \equiv -\frac{d^2\Theta}{db^2}|_{b=b_c}$ as a function of the initial flow velocity v_∞ , for the solar model described in section IV. The strength of the skirt caustic is proportional to $H^{-1/2}$.

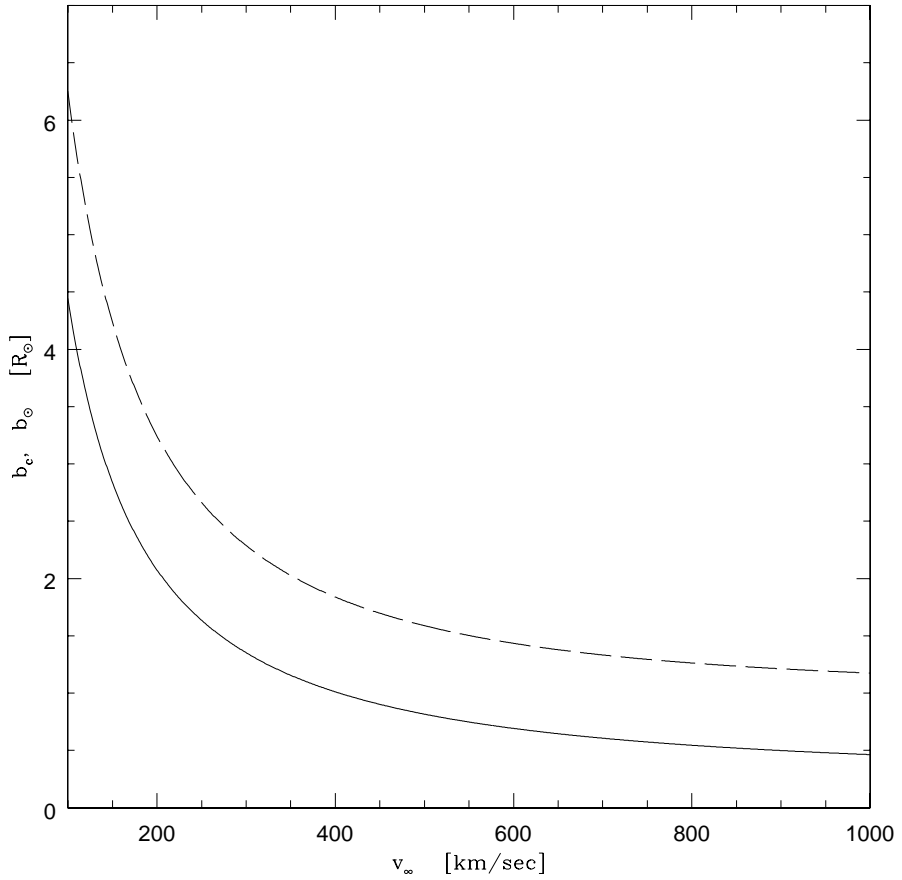


FIG. 6. The impact parameter b_c of the trajectory of maximum scattering angle (solid line) and the impact parameter b_\odot of the grazing trajectory (dashed line) as a function of initial flow velocity v_∞ , for the solar model described in section IV. The strength of the skirt caustic is proportional to b_c .

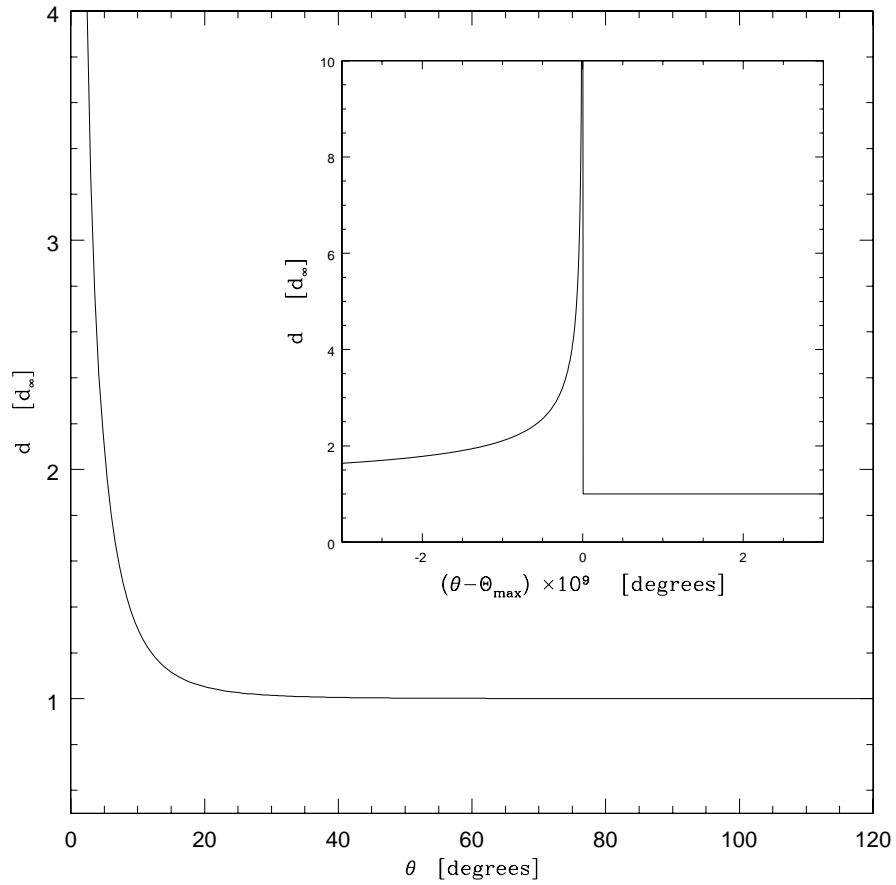


FIG. 7. The density of a cold collisionless flow past the Sun as a function of polar angle for $r = 1$ AU and $v_\infty = 255$ km/s. The divergence at $\theta = 0$ is the spike caustic. The skirt caustic is at $\theta = 115^\circ$. It is invisible on the scale of the main plot but is shown in the inset.

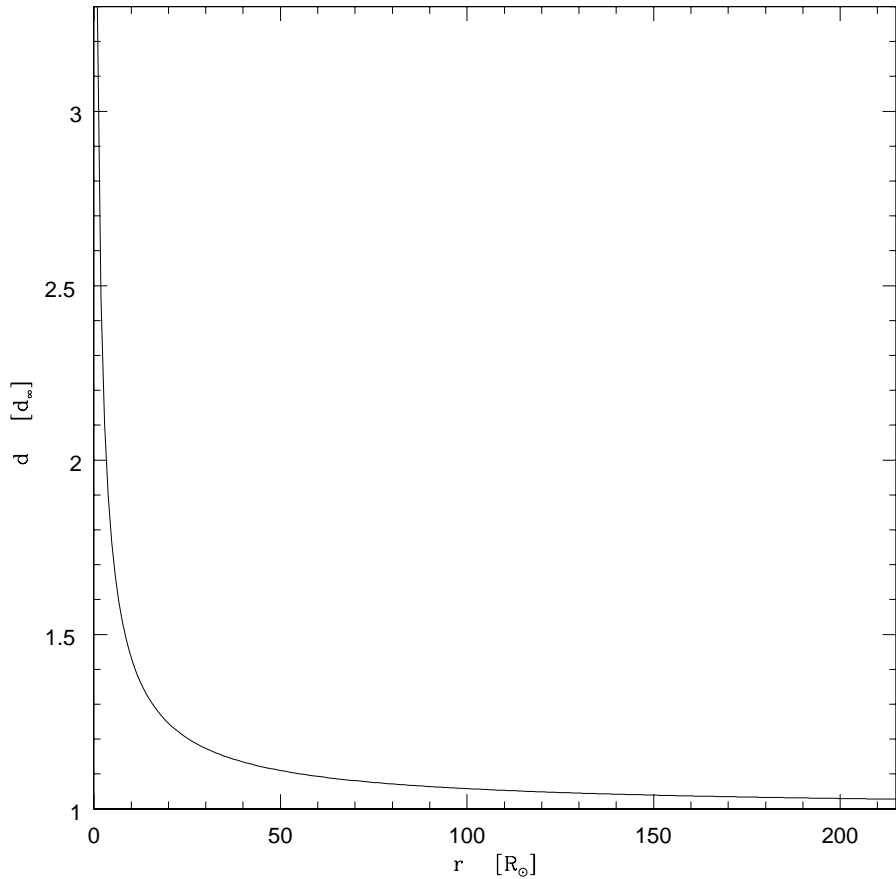


FIG. 8. The density as a function of distance to the Sun, in the isothermal model with $\sqrt{v^2} = 270$ km/s, if the Sun were not moving with respect to the halo ($v_\odot = 0$). The increase in density at small r , compared to d_∞ , is the effect of the Sun's gravity. At the Earth's distance the increase is approximately 3%.

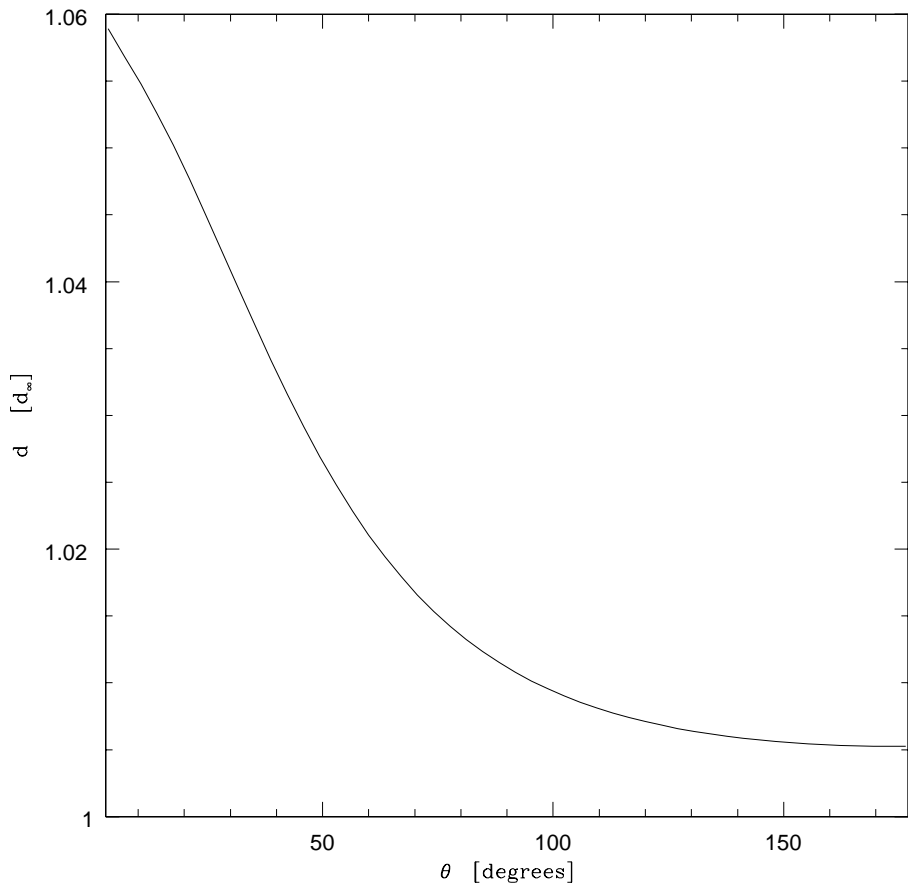


FIG. 9. The density as a function of polar angle θ at $r = 1$ A.U. in the isothermal model with $\sqrt{\vec{v}^2} = 270$ km/s and $v_\odot = 220$ km/s. θ is relative to the direction of $-\vec{v}_\odot$. The Earth's orbit is inclined at approximately 60° relative to \vec{v}_\odot . The annual modulation due to the Sun's gravity can be read off by comparing $\theta \sim 60^\circ$ (March 3) and $\theta \sim 120^\circ$ (September 2). It is approximately 0.7% in amplitude.